PHYSICAL REVIEW D **88,** 045006 (2013)

Probing the Sun's inner core using solar neutrinos: A new diagnostic method

Ilídio Lopes*

Centro Multidisciplinar de Astrofísica, Instituto Superior Técnico, 1049-001 Lisboa, Portugal
and Departamento de Física, Universidade de Évora, 7002-554 Évora, Portugal

(Received 12 February 2013; revised manuscript received 27 June 2013; published 7 August 2013)

The electronic density in the Sun's inner core is inferred from the ^{8}B, ^{7}Be and *pep* neutrino flux measurements of the Super-Kamiokande, SNO and Borexino experiments. We have developed a new method in which we use the KamLAND detector determinations of the neutrino fundamental oscillation parameters: the mass difference and the vacuum oscillation angle. Our results suggest that the solar electronic density in the Sun's inner core (for a radius smaller than 10% of the solar radius) is well above the current prediction of the standard solar model, and by as much as 25%. A potential confirmation of these preliminary findings can be achieved when neutrino detectors are able to reduce the error of the electron-neutrino survival probability by a factor of 15.

DOI: 10.1103/PhysRevD.88.045006 PACS numbers: 26.65.+t, 14.60.Pq, 96.60.Jw

I. INTRODUCTION

Traveling close to the speed of light and with a very large mean free path, solar neutrinos provide a unique and powerful tool to study the properties of the plasma in the Sun's core. During the last two decades, the increase in the number of neutrino detectors, accompanied by a significant improvement in the accuracy of the measurements, has led to major progress in the research field of neutrino physics.

Among many breakthroughs in solar neutrino physics, two are particularly worth mentioning due to their relevance for this work. In 2001, the Sudbury Neutrino Observatory (SNO) experiment [1], following in the footsteps of previous neutrino experiments (e.g., Ref. [2]), definitely confirmed the neutrino flavor oscillations in vacuum and matter. This theoretical model was first suggested by Pontecorvo [3] to explain oscillations in vacuum, and later extended by Wolfenstein [4], Mikheyev and Smirnov [5] to include the oscillations of neutrinos in matter. This is the reason why this last oscillation mechanism is also called the Mikheyev-Smirnov-Wolfenstein (MSW) effect.

In the following year, another important discovery occurred: the Kamiokande Liquid scintillator Anti-Neutrino Detector (KamLAND) [6] measured the flux of antineutrinos from distant reactors, confirming the oscillation nature of neutrinos. Furthermore, KamLAND found that a unique combination of oscillation parameters could explain the neutrino oscillations data, the so-called large mixing angle solution. More significantly, for the first time it was possible to measure the parameters related with the flavor oscillations of neutrinos in vacuum from a source of neutrinos that is not the Sun. The three-flavor neutrino oscillations based only on KamLAND data analysis [7,8] give $\Delta m^2_{21} = 7.49 \pm 0.20 \times 10^{-5}$ eV^2 and $\tan^2\theta_{21} = 0.436 \pm 0.102$. The two-flavor neutrino oscillations data analysis ($\theta_{13} = 0$) gives identical results, but the value of $\tan^2\theta_{21}$ increases by 11%.

Once the fundamental parameters of neutrino flavor oscillations are determined independently of the neutrinos coming from the Sun (at least in the case of the KamLAND experiment), it is reasonable to use, or at least to discuss the possibility of using, solar neutrino flux measurements to probe the Sun's interior. Although our understanding of the basic physical mechanisms occurring inside the Sun is quite robust, there is still a certain number of unknown processes in the solar core that neutrinos could help to resolve (see Ref. [9] and references therein). Furthermore, if we wish to use the Sun as a cosmological tool (e.g., Refs. [10–16]) in an identical manner to how neutron stars (e.g., Refs. [17–21]) are used to constrain the dark matter particle properties, then this will only be possible if we have reliable methods to diagnose the solar core.

Most of the progress achieved in describing accurately the physical processes occurring in the Sun's interior is owed to helioseismology (e.g., Ref. [2]): the present seismic data allows the determination of the sound speed and radial density profiles to be obtained with high accuracy between the solar surface and the first layers of the nuclear region [22,23]. Comparing the present Sun's structure as predicted by the standard solar model (SSM) with the helioseismological data, the sound-speed difference is at most of the order of 2% (mainly in the radiative region), and the density difference is of the order of 10% (in the convective zone). The origin of the sound-speed difference is unknown, probably related to some physical mechanisms occurring during the evolution of the star [9], but the density difference has been linked to a poor description of the solar convection [24,25].

In the last few years, several theoretical models have been put forward to explain this discrepancy between theory and helioseismological data. Most of these proposals are able to reduce the sound-speed difference. Among the various proposals, we choose to mention three

*ilidio.lopes@ist.utl.pt; ilopes@uevora.pt

of them, which are also validated by stellar observations. This is the case with solar models with no standard pre-main-sequence evolution, like solar evolution models that take into account the temporal evolution of the solar internal rotation [26], and solar models for which during a certain period of their pre-main-sequence evolution, the star has its mass changed by a mechanism of mass loss or accretion [27,28].

Another physical process that has been recently considered important for Sun-like stars with planetary systems is the possibility that the star during its formation, or even in its pre-main-sequence phase, could have its internal metallicity increased due to the migration of heavy nuclei from the planetary disk towards the core of the protostar [29]. This scenario has been suggested by recent high-precision spectroscopic observations of solar twins with and without planetary systems [30,31]. In particular, it was found that the former group of stars presents a larger amount of metals in the surface than the latter group. Up to now, how exactly this mechanism operates is still unknown, but it has been shown to be linked to the formation of Earth-like planets. If this process occurs, this could increase significantly the abundances of elements such as carbon, nitrogen and oxygen, increasing the overall metallicity of the stellar interior. Therefore, the amount of heavy elements like carbon, nitrogen and oxygen in the Sun's interior can be well above the values presently measured in the solar photosphere [32]. The observations suggest that stars like the Sun could have a 30% excess of metals in their radiative interior when compared with current values predicted by the standard solar model [2,9]. Furthermore, the sound-speed difference is reduced to a value qualitatively close to the sound-speed difference obtained with the previous metal abundance measurements [33]. This issue is particularly relevant for the neutrinos produced in the nuclear reactions of the carbon-nitrogen-oxygen (CNO) cycle. If the excess in abundances occurs for carbon, nitrogen and oxygen elements, the neutrino fluxes produced in the CNO cycle will be well above the values predicted by the standard solar model [29].

As shown, several physical mechanisms are concurrent with each other towards reducing the sound-speed difference in the solar interior, but the current solar data (including helioseismology data) do not allow us unequivocally to determine which are the best proposals. A strategy going forward to resolve this issue is to investigate new techniques to diagnose the plasma of the solar interior, including the solar inner core. In particular, this would be done by constraining quantities other than the sound-speed profile, such as the electronic density or the plasma density.

Presently, due to the low amount of low-degree acoustic modes, there is still a large uncertainty in the inversion of the sound-speed profile in the solar inner core, and consequently, the seismic diagnostic of this region is quite inaccurate. Even if it is possible to have some information about the sound speed in this region, our knowledge about the local density is much more uncertain. Naturally, the most reliable hope to probe the density in the Sun's core is to use gravity modes, although their existence must still be confirmed [34]. The solar neutrinos are a natural alternative for diagnosing the solar interior, provided that the precision in the measurement of neutrino fluxes is obtained with the required accuracy. If this experimental goal is succeeded, it will provide a major contribution to resolving this problem.

A first attempt to obtain the electronic density in the Sun's interior was made by Balantekin *et al.* [35]. In their work, the authors computed the electronic density as an expansion in powers of the local density plasma, under the hypothesis that neutrino oscillations occur with a small-angle MSW solution. The result obtained allows a relatively good analytical representation of the electronic density in most of the radiative region. The method becomes imprecise only in the core of the Sun below 20% of the solar radius.

Finally, it is worth mentioning that there is still some uncertainty on the basic parameters of neutrino oscillations, which in turn can introduce some uncertainty in the total fluxes of neutrinos of different flavors. However, as was pointed out by Bhat *et al.* [36], this effect is much smaller than the MSW effect discussed in this work. In particular, Balantekin and Malkus [37] have studied the impact of the third neutrino oscillation mixing angle in vacuum on the neutrino flavor oscillations related with matter, and have found that the impact was negligible. A review of the properties of the propagation of neutrinos in matter can be found in Balantekin [38].

In this paper, we focus on the inner nuclear region of the Sun ($r \leq 0.1 R_\odot$), and we will present and discuss a new diagnostic method that constrains the electronic density that comes from current neutrino flux measurements in this region. The method is based in determining the electronic density in the Sun's inner core, as a linear correction to the present values of solar neutrino fluxes obtained for the present standard solar model. What makes this new diagnostic particularly appealing is the possibility of constraining the electronic density at a distance of 5% from the center of the Sun, a very central region which is very difficult to probe by any other methods.

II. THE SOLAR NEUTRINO ENERGY SPECTRUM

Neutrinos are produced in the Sun's interior through several reactions of the nuclear network, usually known as proton-proton (PP) chains and the carbon-nitrogen-oxygen (CNO) cycle. Figure 1 shows the neutrino spectra of our standard solar model [39], computed with an updated version of the stellar evolution code CESAM [40]. This version of CESAM has an up-to-date and very refined microscopic physics (equation of state, opacities, nuclear reaction rates, and an accurate treatment of the microscopic diffusion of heavy elements), including the solar

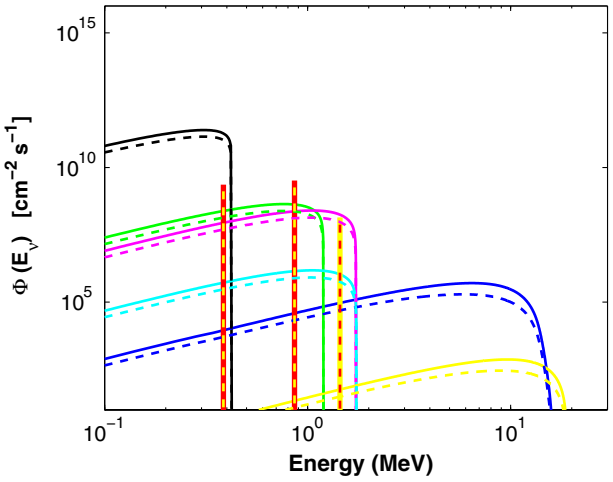

FIG. 1 (color online). The solar neutrino energy spectrum predicted by our standard solar model. The solid curves correspond to the total (electron-flavor) neutrino fluxes produced in the various nuclear reactions of the proton-proton chains and carbon-nitrogen-oxygen cycle. The dashed curves correspond to electron-neutrino fluxes of the various nuclear reactions after neutrino flavor conversion. The color curves define the following neutrino sources from the proton-proton chain reactions: ^{8}B (blue curve), ^{7}Be (two red-yellow lines), *pep* (yellow-red line), *hep* (yellow curve) and *pp* (black curve); and the following neutrino sources from the carbon-nitrogen-oxygen cycle: ^{13}N (green curve), ^{15}O (magenta curve) and ^{17}F (cyan curve). The neutrino fluxes from continuum nuclear sources are given in units of cm^{-2} s^{-1} Mev^{-1}. The line neutrino fluxes are given in cm^{-2} s^{-1}.

mixture of Asplund *et al.* [32] and nuclear reaction rates from the NACRE Compilation [41,42]. The solar models are calibrated to the present solar radius $R_\odot = 6.9599 \times 10^{10}$ cm, luminosity $L_\odot = 3.846 \times 10^{33}$ ergs^{-1}, mass $M_\odot = 1.989 \times 10^{33}$ g, and age $t_\odot = 4.54 \pm 0.04$ Gyr (e.g., Ref. [2]). The models are required to have a fixed value of the photospheric ratio of metal abundance over hydrogen abundance in agreement with the used solar mixture. The total neutrino fluxes (on Earth) predicted by this model are the following: $\phi(pep) = 1.4 \times 10^8$, $\phi(^7\text{Be}) = 4.7 \times 10^9$, $\phi(^8\text{B}) = 5.3 \times 10^6$, $\phi(^{13}\text{N}) = 5.3 \times 10^8$, $\phi(^{15}\text{O}) = 4.5 \times 10^8$, $\phi(^{17}\text{F}) = 5.0 \times 10^6$ and $\phi(pp) = 5.9 \times 10^{10}$, in units of cm^{-2} s^{-1}. This solar model is in agreement with the most current helioseismology data and is identical to others published in the literature (e.g., Refs. [26–28,43]). The neutrino fluxes of ^{8}B, ^{7}Be and *pep* are in agreement with the current solar neutrino experiments. The new NACRE table [41] presents a set of S factors slightly different from previous ones [42], but with a smaller error bar. Therefore, the ^{8}B, ^{7}Be and *pep* total neutrino fluxes are almost the same as those found based on previous predictions; the differences are mainly due to the change in the S factors of a few nuclear reactions like $^3\text{He}(^3\text{He}, 2p)^4\text{He}$ and $^7\text{Be}(p, \gamma)^8\text{B}$. Nevertheless, the standard solar model computed with this new set of laboratory cross-section measurements [41] predicts solar neutrino fluxes in excellent agreement with experimental data [44]. Moreover, the impact of this update of the NACRE table on the Sun's core electronic density is negligible, because the ratios of neutrino flavor fluxes are almost independent of the total neutrino flux for each neutrino source.

Figure 2 shows the different neutrino emission sources inside the Sun. The nuclear reactions are ordered inside the Sun according to the temperature required for the fusion reaction between reacting nuclei to occur. Naturally, the nuclear reactions between heavy nuclei are located nearer the center than reactions between lighter nuclei. In Fig. 2, we show the electron-neutrino source function $\Phi(r)$ related to the electron neutrinos produced in the *PP* chain (*pp*, *pep*, ^{8}B and ^{7}Be) and CNO cycle (^{13}N, ^{15}O, ^{17}F) nuclear reactions.

The neutrino sources produced by the nuclear reactions of the *PP* chain are located between the center and 30% of the solar radius. The *pp* neutrino source extends from the center up to 30% of the solar radius with its maximum located at 10% of the solar radius. The other *PP* chain neutrino sources are *pep*, ^{7}Be and ^{8}B and have emission shells with widths of 22%, 18% and 10%, respectively, and maximums occurring at 8.6%, 5.8% and 4.5% of the solar radius, respectively. In particular, it is worth noticing that the *pp* and *pep* nuclear reactions are strongly dependent on

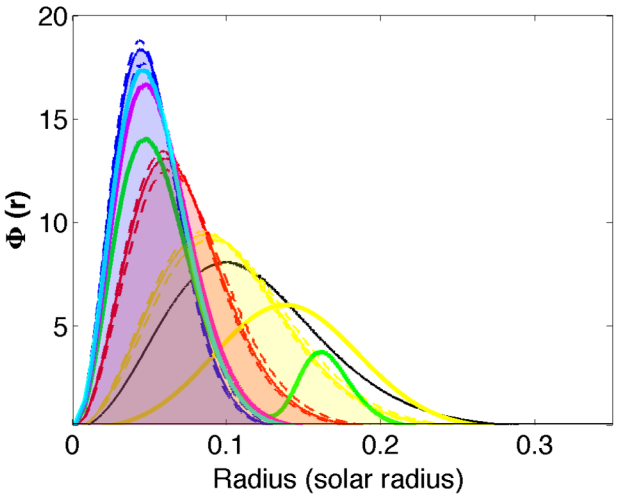

FIG. 2 (color online). The electron-neutrino fluxes produced in the various nuclear reactions. The $\Phi(r)$ for which neutrino fluxes have been measured experimentally (^{8}B, ^{7}Be and *pep*) are indicated with a shaded area. If the central temperature of the standard solar model changes by +2.5% (−4%) and density changes accordingly (+ 7.4% and −12.7%) to keep the energetic balance, the neutrino fluxes change by +70% (− 60%) for ^{8}B, by 30% (−38%) for the ^{7}Be neutrino emission lines, and by 13% (− 20%) for the *pep* emission line. The function $\Phi(r)$ for these two cases is indicated by dashed curves. The color scheme is the same as for Fig. 1. In particular, ^{7}Be (two red-yellow lines) and *pep* (yellow-red line) in Fig. 1 correspond to this figure's red and yellow shaded areas, respectively.

the total luminosity of the star. Similarly, the neutrino sources related with the CNO cycle of nuclear reactions (cf. Fig. 2), ^{15}O, ^{17}F and ^{13}N neutrinos, occur in emission shells with a width of 16% of the solar radius. The maximum neutrino production of these sources occurs at 5% of the solar radius. ^{13}N neutrinos have a second emission shell located between 12% and 25% of the Sun's radius, with its maximum occurring at 16% of the solar radius.

It is important to note that an increase or decrease of the temperature in the core of the Sun (caused by the presence of some known or unknown physical process) does not change much the location of the neutrino emission region $\Phi(r)$, even if the total neutrino fluxes change significantly (cf. Fig. 2). This is due to the strong dependence of neutrino nuclear reactions on the temperature.

In the case of solar models for which the central temperature is changed by a few percent, the neutrino emission regions (i.e., the ^{8}B,^{7}Be and *pep* neutrino emission regions among others) does not change much, although the total neutrino fluxes are strongly affected. The position of the maximum of $\Phi(r)$ of the different neutrino sources changes by less than 1%.

III. NEUTRINO FLAVOR OSCILLATIONS

The theory of neutrino flavor oscillations (i.e., Ref. [45]) describes the propagation of neutrinos in space [3] and the interaction of neutrinos with matter [4,5]. Yuksel [46] showed that the survival probability of solar neutrinos calculated in a model with two-flavor neutrino oscillations or three-flavor neutrino oscillations have very close values.

In the Sun, the electron-neutrino survival or appearance probabilities depend only on three fundamental oscillation parameters: the mass difference Δm_{12} and the angles θ_{21} and θ_{13}. In the absence of the MSW effect caused by the Earth's globe, the survival probability during the day of a three-flavor neutrino oscillation can be reduced to a modified two-flavor neutrino oscillation model that is accurately described as

$$P_{\nu_e}(E_\nu, r) = \cos^4\theta_{13} P_{2\nu_e}(E_\nu, r) + \sin^4\theta_{13}, \quad (1)$$

where E_ν is the energy of the neutrino and $P_{2\nu_e}(E_\nu, r)$ is the probability in the case of a two-flavor oscillation model (e.g., Refs. [7,45,47]). $P_{2\nu_e}(E_\nu, r)$ is given by

$$P_{2\nu_e}(E_\nu, r) = \frac{1}{2} + \frac{1}{2}\cos(2\theta_{21})\cos(2\theta_m), \quad (2)$$

where θ_m is the mixing angle at the production source inside the Sun. In the derivation of this formula it was assumed that the first-order correction to the propagation of neutrinos in matter is valid once the adiabatic condition is verified in the radiative region of the solar interior [47,48]. The phase θ_m is the most important term in this analysis, since it depends on the electron density of the Sun's core. The mixing angle θ_m is given by

$$\sin(2\theta_m) = \frac{\sin(2\theta_{12})}{\sqrt{(V_m - \cos(2\theta_{12}))^2 + \sin^2(2\theta_{12})}}, \quad (3)$$

where V_m is a function of solar radius. The values of Δm^2_{12} and θ_{21} can be solely determined from neutrino experiments (not using the neutrinos coming from the Sun), such as the KamLAND reactor experiment [6]. V_m is a function of solar plasma density, given by

$$V_m(E_\nu, r) = 2\sqrt{2} G_f n_e(r) E_\nu \cos^2(\theta_{13})/\Delta m_{21}, \quad (4)$$

where G_f is the Fermi constant and $n_e(r)$ is the electron density of plasma. The electron density $n_e(r) = N_o\rho(r)/\mu_e(r)$, where $\mu_e(r)$ is the mean molecular weight per electron, $\rho(r)$ is the density of matter in the solar interior, and N_o is Avogadro's number.

The radial neutrino emission profile of electron neutrinos is specific for each nuclear reaction (cf. Fig. 2). It follows that the average survival probability of electron neutrinos for each of the emission neutrino sources, $\langle P_{\nu_e}(E_\nu)\rangle$, is given by

$$\langle P_{\nu_e}(E_\nu)\rangle = A^{-1}\int P_{\nu_e}(E_\nu, r)\Phi(r)4\pi\rho(r)r^2 dr, \quad (5)$$

where $A = \int \Phi(r)4\pi\rho(r)r^2 dr$ is a normalization constant. In the following, $\langle\cdots\rangle$ defines the $\Phi(r)$ weight average of a certain quantity, as defined in the previous equation.

The electron-neutrino survival probability functions $\langle P_{\nu_e}(E_\nu)\rangle$ for different nuclear reactions are shown in Fig. 3. The survival probabilities of electron neutrinos were computed by using the fundamental parameters of solar neutrino oscillations in vacuum—namely Δm_{12} and θ_{12}, as determined by the KamLAND experiment [7]. Although the contribution related to θ_{13} is minor, we take its contribution into account by choosing $\theta_{13} = 9$ deg , a value that is in agreement with current experimental measurements, $8.96^{+0.45}_{-0.51}$ deg [49] and $9.06^{+0.50}_{-0.57}$ deg [50]. Furthermore, Balantekin and Malkus [37] have shown that the electron-neutrino survival probability functions are not very sensitive to the mixing θ_{13} for the neutrino energy range where the MSW effect is dominant, at least in the energy range where the neutrino flux measurements are taken.

Since electron neutrinos are produced in nuclear reactions located at different distances from the center, there is a clear differentiation between the different survival probability curves (cf. Fig. 3). Nevertheless, for neutrinos with low or high energy, these curves become indistinguishable, as low-energy neutrinos are affected only by vacuum fluctuations, and high-energy neutrinos are affected by a cumulative effect of vacuum oscillations and matter oscillations. It is worth noticing that the possibility of observing the MSW effect on solar neutrinos is limited, as the neutrino flavor oscillations induced by matter depend on the neutrino emission spectrum (cf. Fig. 1) and on the location of the neutrino source in the Sun's core (cf. Fig. 2).

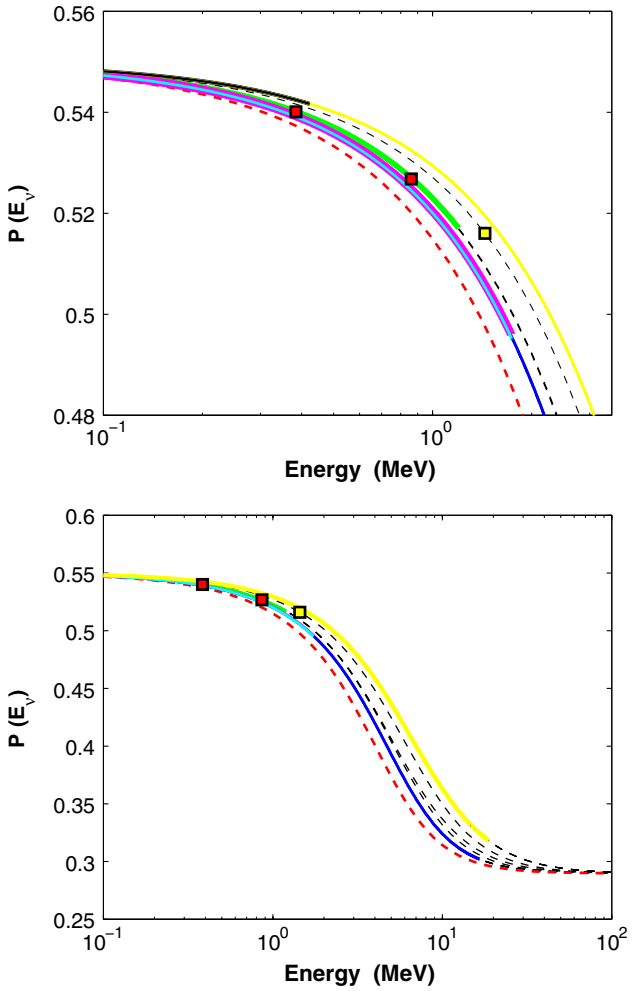

FIG. 3 (color online). The survival probability of electron-neutrinos in function of the neutrino energy. The reference curve (red dashed curve) defines the survival probability of electron-neutrinos in the centre of the Sun. The colored parts of the curves indicate the energy range of neutrinos produced in the Sun's core for each nuclear reaction (cf. Fig. 1).

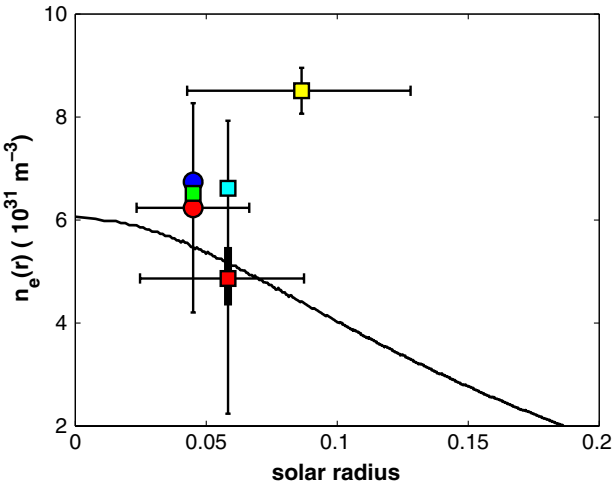

FIG. 4 (color online). The core of the Sun: the radial profile of electronic density (black continuous curve). The points shown correspond to the values of the electronic density *inverted*, $n_e(\bar{r})$, for the values of $\bar{r}$, $0.045R_\odot$, $0.058R_\odot$ and $0.086R_\odot$ computed from the survival probability of electron neutrinos for ^{8}B, ^{7}Be and *pep* neutrino fluxes (see Table I). (a) ^{8}Be *neutrino flux*: Averaged $P_{\nu_e}(^8\mathrm{B})$ (red sphere), $P_{\nu_e}(^8\mathrm{B}) = 0.32 \pm 0.05$ (SNO, blue sphere), $P_{\nu_e}(^8\mathrm{B}) = 0.32 \pm 0.12$ (Borexino, green square). (b) ^{7}Be *and pep neutrino fluxes* (Boroxino experiment): (i) The $P_{\nu_e}(pep) = 0.62 \pm 0.17$ (yellow square) [53]. (ii) The $P_{\nu_e}(^7\mathrm{Be}) = 0.52^{+0.07}_{-0.06}$ (red square) and $P_{\nu_e}(^7\mathrm{Be}) = 0.56^{+0.10}_{-0.10}$ (cyan square) [51,52]. The electronic densities inverted from the ^{8}B (red circle) and *pep* (yellow square) neutrino fluxes were computed assuming that the current vertical errors of $P_{\nu_e}(^8B)$ and $P_{\nu_e}(pep)$ were reduced by a factor of 15. In the case of the ^{7}Be (red square) neutrino flux, this was computed using the real vertical error bar—the thicker bar here corresponds to a reduction of the current error by a factor of 5.

The parts of the survival probability of electron neutrinos that can be measured by solar neutrino experiments are shown in Fig. 3. In particular, we notice that the ^{8}B neutrino flavor oscillation is strongly dependent on the MSW effect, specially for neutrinos with a higher energy. However, the ^{7}Be neutrino flux is much less dependent on the MSW effect, particularly the ^{7}Be neutrino flux corresponding to the line of lower energy. Similarly, the *pep* neutrino flux is also weakly dependent on the MSW effect. Accordingly, the constraint obtained in the electronic density from the ^{8}B neutrino flux measurement is much more reliable than the constraint obtained from ^{7}Be and *pep* neutrino flux measurements (cf. Fig. 3). Furthermore, it is worth noticing a second-order effect. The conversion of electron neutrinos due to matter oscillations depends on the local electron density $n_e(r)$: a decrease of the central density of $n_e(r = 0)$ moves all the $\langle P_{\nu_e}(E_\nu)\rangle$ of different neutrino sources to the right, and a rapid variation of $n_e(r)$ (possibly caused by a rapid variation of density) with the radius increases the distance between the consecutive $\langle P_{\nu_e}(E_\nu)\rangle$ curves (cf. Fig. 3).

Once the fundamental parameters of solar neutrino oscillations in vacuum are known and determined independently from solar neutrino fluxes, in principle, the probability of survival of electron-flavor solar neutrinos can be used to infer the radial electronic density profile in different locations of the solar core. By perturbation analysis of Eqs. (1)–(5), the value of the electronic n is determined for each value of the survival probability of electron neutrinos obtained from the experimental neutrino data [39]. The procedure is as follows: for neutrinos of a given energy E_ν, the electronic density correction Δn is computed from the standard solar model electronic density n_o as $\Delta n/n_o = \beta_o \Delta P/P_o$, with $\Delta P = \bar{P} - P_o$, where P_o and $\bar{P}$ are the survival probabilities of electron neutrinos obtained from the standard solar model and experimental data. β_o is a coefficient computed from the standard solar model data. It follows that the new value of electronic density, $\bar{n}_e$, is

obtained as $\bar{n}_e = n_o + \Delta n$. Figure 4 shows the inverted electronic density values obtained from the survival probability of electron neutrinos computed from experimental data.

IV. SOLAR NEUTRINO FLUXES

Usually, the fluxes of the different neutrino flavors are represented by Φ_t for the total neutrino flux, Φ_e for the electron-neutrino flux, and $\Phi_{\tau\mu}$ for the nonelectron flavor component of neutrinos, corresponding to the experimentally indistinguishable flavors of τ and μ neutrinos [45]. It follows that $\Phi_t = \Phi_e + \Phi_{\tau\mu}$. Such quantities are computed from the measured neutrino fluxes that result from the interaction of neutrinos with the detector, which occur through three different interaction processes. As for the charged-current reaction (CC) of neutrinos with a deuterium nucleus and the elastic scattering (ES) of neutrinos off electrons, both processes are observed through the detection of the Cherenkov light produced by electrons in the heavy water. A third process known as neutral-current (NC) reaction is observed via the detection of neutrons. Conveniently, such neutrino fluxes are called $\Phi_{\rm CC}$, $\Phi_{\rm ES}$ and $\Phi_{\rm NC}$. Φ_t is determined as $\Phi_t = \Phi_{\rm NC}$, once the neutral-curent reaction is sensitive to all flavors of neutrinos. The flux of electron-neutrinos is measured by the charged-current reaction $\Phi_e = \Phi_{\rm CC}$, or alternatively it can be measured by the neutrino-electron scattering (ES), for which Φ_e is computed as $\Phi_e = 1.2\Phi_{\rm ES} - 0.20\Phi_{\rm NC}$.

Among current solar neutrino experiments, the measurements of ^{8}B neutrino flavors are the most compelling because for ^{8}B neutrinos, unlike in the case of ^{7}Be and *pep* neutrinos [51–53], the measurements allow the computation of Φ_t and Φ_e for different and independent solar experiments. Furthermore, ^{8}B neutrino flux is much more sensitive to the density stratification of the solar core—i.e., the neutrino flavor oscillation induced by the MSW effect—than other sources of neutrino fluxes such as ^{7}Be and *pep* neutrinos. This allows us to make an estimation of the survival probability of electron-neutrino flavors independent of solar models and neutrino oscillation models (see Table I). $\Phi_t(^8\mathrm{B})$ is estimated by the Sudbury Neutrino Observatory (SNO phase III) experiment [54] from $\Phi_{\rm NC}(^8\mathrm{B})$, a value 7% larger than the previous SNO measurement [58]. The SNO Collaboration have performed another measurement [59] of $\Phi_{\rm NC}(^8\mathrm{B})$ by enhancing the sensitivity of heavy water to neutral current interaction (Enhanced NC).

In Table I we show the electron-neutrino flux $\Phi_e(^8\mathrm{B})$ estimated from the SNO, Super-Kamiokande and Borexino measurements [55–57]. Although the errors in most of the neutrino-measured fluxes are still quite significant, it is encouraging to observe that the different experiments lead to quite identical values of $\Phi_e(^8\mathrm{B})$. The $\Phi_{\rm ES}(^8\mathrm{B})$ computed in the case of SNO phase III predicts a value 4% lower that in the case of SNO enhanced NC. The survival probability of electron neutrinos $P_{\nu_e}(^8\mathrm{B})$ was computed as the ratio $\Phi_e(^8\mathrm{B})/\Phi_t(^8\mathrm{B})$ [60]. The error is obtained by adding up the errors quadratically. The values of $P_{\nu_e}(^8\mathrm{B})$ are quite similar for all experiments with a difference smaller than 17% (cf. Table I). In particular, the value of the Borexino data (SNO phase III), $P_{\nu_e}(^8\mathrm{B}) = 0.32 \pm 0.12$, is 9% higher than the estimation made by the Borexino Team [56], which obtained a value $P_{\nu_e}(^8\mathrm{B}) = 0.29 \pm 0.1$ at the mean energy of 8.9 MeV. The averaged value of all the experiments, $P_{\nu_e}(^8\mathrm{B})$, is estimated to be 0.32 ± 0.20. Figure 4 shows the *inverted* electronic density $\bar{n}_e(\equiv n_e(\bar{r}))$ at different locations of the solar radius, computed as described in the previous section. The theoretical

TABLE I. ^{8}B neutrino fluxes and electron-neutrino survival probabilities.

Experiment [$\Phi_{\rm NC}$] 10^6 cm^{-2} s^{-1}	$\Phi_{\rm CC}$ or $\Phi_{\rm ES}$ 10^6 cm^{-2} s^{-1}	Φ_e 10^6 cm^{-2} s^{-1}	P_{ν_e}
SNO (Phase III)			
5.54 ± 0.69			
SNO (Phase III)[a]	*CC*: 1.67 ± 0.12	1.67 ± 0.12	0.30 ± 0.04
SNO (Phase II)[b]	*CC*: 1.76 ± 0.14	1.76 ± 0.14	0.32 ± 0.05
Borexino[c]	*ES*: 2.4 ± 0.5	1.77 ± 0.62	0.32 ± 0.12
SK (Phase III)[d]	*ES*: 2.32 ± 0.09	1.67 ± 0.18	0.30 ± 0.05
SNO (Enhanced NC)			
5.21 ± 0.65			
SNO (Phase III)	*CC*: 1.67 ± 0.12	1.67 ± 0.12	0.32 ± 0.05
SNO (Phase II)	*CC*: 1.76 ± 0.14	1.76 ± 0.14	0.34 ± 0.05
Borexino	*ES*: 2.4 ± 0.5	1.84 ± 0.61	0.35 ± 0.13
SK (Phase III)	*ES*: 2.32 ± 0.09	1.74 ± 0.17	0.33 ± 0.05
Mean value	...	...	0.32 ± 0.20

[a]Aharmim *et al.* [54].
[b]Aharmim *et al.* [55].
[c]Bellini *et al.* [56].
[d]Abe *et al.* [57].

value P_o was estimated for neutrinos with energy above 5 MeV in the case of ^{8}B neutrinos, and for the values of 0.862 and 1.44 MeV for ^{7}Be and *pep* neutrinos. In Fig. 4, for reasons of clarity, the error bars are shown only in three cases. In all these data points, the length of the *horizontal error bar* of each inverted data point $\bar{n}_e$ (of a specific $\bar{r}$) defines the radial interval where 68.2% (equivalent to one σ, in a normal distribution) of the neutrino flux is produced.

The mean value of $P_{\nu_e}(^8\mathrm{B})$ and most of the individual values suggest that the electronic density in the core of the Sun is at least 25% higher than in the current solar model (cf. Table I and Fig. 4). The high value of $P_{\nu_e}(pep)$ obtained by the Borexino Team reinforces the high value of $n_e(r)$ in the core. Although the present value of $P_{\nu_e}(^7\mathrm{Be})$ is in agreement with the standard solar model, the previous determination $P_{\nu_e}(^7\mathrm{Be})$ also suggests a high value of $n_e(r)$ in the core. Nevertheless, it should be noticed that both electronic density values obtained from *pep* and ^{7}Be survival electron-neutrino probabilities depend on the solar model (contrarily to ^{8}B), and therefore have a limited diagnostic capability.

A potential confirmation of our findings can be achieved as the experimental error in the neutrino measurements decreases and levels of accuracy significantly increase. As per Fig. 4, a clear insight will be possible if the error in the determination of the electron-neutrino survival probability obtained from the present measurements can be reduced by a factor of 15.

V. SUMMARY AND CONCLUSION

We show that if the fundamental parameters of neutrino oscillations are determined from Earth's neutrino detector flux measurements, as per the KamLAND experiment, then the solar neutrino fluxes can be used to invert the electronic density in the Sun's inner core. In this work we have developed a new method to infer the electronic density based in this principle. The method consists in determining the *real* electronic density of the solar core (in function of the radius) as a small correction to the electronic density predicted by the standard solar model.

All the observed neutrino fluxes, i.e., the ^{8}B, ^{7}Be and *pep* neutrino fluxes, have neutrino emission sources located within 10% of the solar radius. Although the accuracy of the current neutrino flux measurements is low, we have found that a significant improvement in the accuracy of these measurements will allow the determination of the electronic density in the Sun's inner core with an error smaller than a few percent. In particular, the reduction of the error bar of the ^{7}Be electron-neutrino survival probability by a factor of 5 allows the determination of the electronic density with an error of 3% (cf. Fig. 4). The measurements of *hep*, ^{13}N, ^{15}O and ^{17}F neutrino fluxes will also contribute significantly to improve the quality of inversion of the electronic density in the Sun's core. In particular, ^{8}B and *hep* high-energy neutrino fluxes are very sensitive to matter oscillations (cf. Fig. 3). Therefore, accurate measurements of these neutrino fluxes will also put stringent constraints on the electronic density in the Sun's core.

This diagnostic of the electronic density of the Sun's inner core combined with the accurate determination of the abundances of heavy elements such as carbon, nitrogen and oxygen from the neutrino fluxes produced in the CNO cycle provides presently the best way to probe the physics of the Sun's inner core. This possibility will become feasible with the upgrade of experiments such as Borexino and the Sudbury Neutrino Observatory (SNO +) [61], as well as the new solar neutrino detector Low Energy Neutrino Astrophysics (LENA) [62].

ACKNOWLEDGMENTS

This work was supported by grants from "Fundação para a Ciência e Tecnologia" and "Fundação Calouste Gulbenkian."

[1] Q. R. Ahmad *et al.*, Phys. Rev. Lett. **87**, 71301 (2001).
[2] S. Turck-Chieze and S. Couvidat, Rep. Prog. Phys. **74**, 086901 (2011).
[3] B. Pontecorvo, Sov. Phys. JETP **6**, 429 (1958).
[4] L. Wolfenstein, Phys. Rev. D **17**, 2369 (1978).
[5] S. P. Mikheyev and A. Y. Smirnov, Nuovo Cimento Soc. Ital. Fis. C **9C**, 17 (1986).
[6] K. Eguchi *et al.*, Phys. Rev. Lett. **90**, 21802 (2003).
[7] A. Gando *et al.*, Phys. Rev. D **83**, 52002 (2011).
[8] S. Abe *et al.*, Phys. Rev. Lett. **100**, 221803 (2008).
[9] S. Turck-Chieze and I. Lopes, Res. Astron. Astrophys. **12**, 1107 (2012).
[10] I. Lopes and J. Silk, Astrophys. J. **752**, 129 (2012).
[11] I. Lopes and J. Silk, Science **330**, 462 (2010).
[12] I. Lopes and J. Silk, Astrophys. J. Lett. **722**, L95 (2010).
[13] M. Taoso, F. Iocco, G. Meynet, G. Bertone, and P. Eggenberger, Phys. Rev. D **82**, 083509 (2010).
[14] D. T. Cumberbatch, J. A. Guzik, J. Silk, L. S. Watson, and S. M. West, Phys. Rev. D **82**, 103503 (2010).
[15] I. P. Lopes, J. Silk, and S. H. Hansen, Mon. Not. R. Astron. Soc. **331**, 361 (2002).
[16] I. P. Lopes and J. Silk, Phys. Rev. Lett. **88**, 151303 (2002).
[17] C. Kouvaris, Phys. Rev. Lett. **108**, 191301 (2012).

[18] C. Kouvaris and P. Tinyakov, Phys. Rev. D **83**, 083512 (2011).
[19] C. Kouvaris and P. Tinyakov, Phys. Rev. Lett. **107**, 091301 (2011).
[20] C. Kouvaris and P. Tinyakov, Phys. Rev. D **82**, 063531 (2010).
[21] C. Kouvaris and P. Tinyakov, arXiv:1212.4075.
[22] S. Basu, W. J. Chaplin, Y. Elsworth, R. New, and A. M. Serenelli, Astrophys. J. **699**, 1403 (2009).
[23] S. Turck-Chieze *et al.*, Sol. Phys. **175**, 247 (1997).
[24] W. P. Abbett, M. Beaver, B. Davids, D. Georgobiani, P. Rathbun, and R. F. Stein, Astrophys. J. **480**, 395 (1997).
[25] Å. Nordlund, R. F. Stein, and M. Asplund, Living Rev. Solar Phys. **6**, 2 (2009).
[26] S. Turck-Chieze, A. Palacios, J. P. Marques, and P. A. P. Nghiem, Astrophys. J. **715**, 1539 (2010).
[27] J. A. Guzik and K. Mussack, Astrophys. J. **713**, 1108 (2010).
[28] A. M. Serenelli, W. C. Haxton, and C. Pena-Garay, Astrophys. J. **743**, 24 (2011).
[29] I. Lopes and J. Silk, Mon. Not. R. Astron. Soc. (to be published).
[30] J. Meléndez, M. Asplund, B. Gustafsson, and D. Yong, Astrophys. J. Lett. **704**, L66 (2009).
[31] I. Ramirez, J. Meléndez, and M. Asplund, Astron. Astrophys. **508**, L17 (2009).
[32] M. Asplund, N. Grevesse, A. J. Sauval, and P. Scott, Annu. Rev. Astron. Astrophys. **47**, 481 (2009).
[33] N. Grevesse and A. J. Sauval, Space Sci. Rev. **85**, 161 (1998).
[34] S. Turck-Chieze *et al.*, Astrophys. J. **604**, 455 (2004).
[35] A. B. Balantekin, J. F. Beacom, and J. M. Fetter, Phys. Lett. B **427**, 317 (1998).
[36] C. M. Bhat, P. C. Bhat, M. Paterno, and H. B. Prosper, Phys. Rev. Lett. **81**, 5056 (1998).
[37] A. B. Balantekin and A. Malkus, Phys. Rev. D **85**, 013010 (2012).
[38] A. B. Balantekin, Phys. Rep. **315**, 123 (1999).
[39] I. Lopes and S. Turck-Chieze, Astrophys. J. **765**, 14 (2013).
[40] P. Morel, Astron. Astrophys. Suppl. Ser. **124**, 597 (1997).
[41] E. G. Adelberger *et al.*, Rev. Mod. Phys. **83**, 195 (2011).
[42] C. Angulo *et al.*, Nucl. Phys. **A656**, 3 (1999).
[43] A. M. Serenelli, S. Basu, J. W. Ferguson, and M. Asplund, Astrophys. J. Lett. **705**, L123 (2009).
[44] A. Serenelli, C. Pena-Garay, and W. C. Haxton, Phys. Rev. D **87**, 043001 (2013).
[45] S. Bilenky, *Introduction to the Physics of Massive and Mixed Neutrinos* (Springer, New York, 2010).
[46] A. B. Balantekin and H. Yuksel, Phys. Rev. D **68**, 113002 (2003).
[47] L. Landau and L. Rosenkewitsch, Z. Phys. **78**, 847 (1932).
[48] C. Zener, Proc. R. Soc. A **137**, 696 (1932).
[49] G. L. Fogli, E. Lisi, A. Marrone, D. Montanino, A. Palazzo, and A. M. Rotunno, Phys. Rev. D **86**, 013012 (2012).
[50] D. V. Forero, M. Tórtola, and J. W. F. Valle, Phys. Rev. D **86**, 073012 (2012).
[51] G. Bellini *et al.*, Phys. Rev. Lett. **107**, 141302 (2011).
[52] C. Arpesella *et al.*, Phys. Rev. Lett. **101**, 91302 (2008).
[53] G. Bellini *et al.*, Phys. Rev. Lett. **108**, 51302 (2012).
[54] B. Aharmim *et al.*, arXiv:1107.2901.
[55] B. Aharmim *et al.*, Phys. Rev. C **75**, 45502 (2007).
[56] G. Bellini *et al.*, Phys. Rev. D **82**, 33006 (2010).
[57] K. Abe *et al.*, Phys. Rev. D **83**, 52010 (2011).
[58] B. Aharmim *et al.*, Phys. Rev. C **81**, 55504 (2010).
[59] S. N. Ahmed *et al.*, Phys. Rev. Lett. **92**, 181301 (2004).
[60] V. Berezinsky and M. Lissia, Phys. Lett. B **521**, 287 (2001).
[61] J. Maneira, Nucl. Phys. B, Proc. Suppl.**217**, 50 (2011).
[62] M. Wurm *et al.*, Astropart. Phys. **35**, 685 (2012).